Numerical Prediction of Subsonic Turbulent Flows over Slender Bodies at High Incidence

David Degani*
Technion—Israel Institute of Technology, Haifa 32000, Israel
and
Lewis B. Schiff† and Yuval Levy‡
NASA Ames Research Center, Moffett Field, California 94035

The physical aspects governing accurate numerical simulation of turbulent flows having large regions of crossflow separation are re-examined. Time-accurate, three-dimensional fine-grid Navier-Stokes solutions were obtained for turbulent subsonic flows over a slender ogive-cylinder body of revolution at large angles of attack. These flowfields are complex and contain regions of crossflow separation and an organized leeward-side vortex structure. An algebraic eddy-viscosity turbulence model has been modified to correctly account for the effects of the vortices on the underlying viscous layers. The numerical results show that the vortical flow structure of subsonic and supersonic high-incidence flows are similar, and can be accurately treated by the modified turbulence model. As the angle of attack is increased, the effectiveness of the model increases since the influence of the vortices on the underlying boundary layer decreases.

Introduction

COMPUTATION of flow over bodies at large angles of attack is a difficult, but significant, problem in aerodynamics. High-angle-of-attack flow is governed by large regions of three-dimensional separated flow, where the boundary layers leave the surface of the body along lines of separation, and roll up on the leeward side of the body to form strong, concentrated vortical flows. Separated flows have historically been treated by a wide variety of computational methods, ranging from potential flow methods, vortex cloud methods, inviscid panel methods incorporating free shear layers, Euler methods, and most recently, parabolized Navier-Stokes (PNS) and time-marching Navier-Stokes techniques. In addition, a variety of combined inviscid/viscous techniques (potential/boundary layer or Euler/boundary-layer techniques) have been utilized. However, it is recognized that the need to account computationally for the close coupling that exists between the strength and location of the leeward vortical flow and the location of the viscous layer separation lines has precluded accurate predictions of high-incidence flow with other than Navier-Stokes techniques.

The introduction of recent supercomputers such as the CRAY-2 has permitted a quantum increase in the size of computational grids. As a result, it is now possible to compute subsonic high-angle-of-attack flows over bodies and aircraft components with codes based on the time-dependent form of the Reynolds-averaged Navier-Stokes equations, and using sufficient grid points to adequately resolve the main features of the three-dimensional separated flow (cf. Refs. 1–5).

Presented as Paper 90-0096 at the AIAA 28th Aerospace Sciences Meeting, Reno, NV, Jan. 8–11, 1990; received March 23, 1990; revision received Dec. 14, 1990; accepted for publication Dec. 24, 1990.

*Associate Professor, Faculty of Mechanical Engineering. Associate Fellow AIAA.
†Special Assistant for High Alpha Technology, Fluid Dynamics Division. Associate Fellow AIAA.
‡Graduate Student, Stanford University. Member AIAA.

In previous work, Degani and Schiff[6,7] developed a modification to the widely used Baldwin-Lomax eddy-viscosity turbulence model that rationally accounts for the presence of the leeward-side vortex structure. Results for supersonic high-incidence turbulent flow, obtained using a parabolized Navier-Stokes method[8] and the modified turbulence model, were compared to experimental measurements. It was shown that accurate computation of high-angle-of-attack supersonic flow can be achieved by 1) use of grid resolutions adequate to resolve the details of both the viscous boundary layers and the off-surface vortical flow, and 2) for turbulent flows, use of the modified turbulence model that accounts for the vortical flow structure.

In the current work, we re-examine the physical assumptions on which the modified eddy-viscosity model is based, and investigate its ability to treat subsonic as well as supersonic high-incidence turbulent flows. We utilize a time-marching thin-layer Navier-Stokes code[9] to compute a series of subsonic laminar and turbulent flows over an ogive-cylinder at $M_\infty = 0.2$. These results are compared to experimental surface pressure distributions, and again demonstrate that accurate computation of high-angle-of-attack flows are dependent on the use of the modified model for turbulent cases.

Theoretical Background

Governing Equations

The conservation equations of mass, momentum, and energy can be represented in a flux-vector form that is convenient for numerical simulation as[10]

$$\partial_\tau \hat{Q} + \partial_\xi(\hat{F} + \hat{F}_v) + \partial_\eta(\hat{G} + \hat{G}_v) + \partial_\zeta(\hat{H} + \hat{H}_v) = 0 \quad (1)$$

where τ is the time and the independent spatial variables, ξ, η, and ζ are chosen to map a curvilinear body-conforming grid into a uniform computational space. In Eq. (1), $\hat{Q}$ is the vector of dependent flow variables; $\hat{F} = \hat{F}(\hat{Q})$, $\hat{G} = \hat{G}(\hat{Q})$, and $\hat{H} = \hat{H}(\hat{Q})$ are the inviscid flux vectors, while the terms $\hat{F}_v$, $\hat{G}_v$, and $\hat{H}_v$ are fluxes containing the viscous derivatives. A nondimensional form of the equations is used throughout this work. The conservative form of the equations is maintained chiefly to capture the Rankine-Hugoniot shock jump relations (where applicable) as accurately as possible.

For body-conforming coordinates and high-Reynolds number flow, if ζ is the coordinate leading away from the surface, the thin-layer approximation can be applied, which yields[11,12]

$$\partial_\tau \hat{Q} + \partial_\xi \hat{F} + \partial_\eta \hat{G} + \partial_\zeta \hat{H} = Re^{-1} \partial_\zeta \hat{S} \qquad (2)$$

where only viscous terms in ζ are retained. These have been collected into the vector $\hat{S}$ and the nondimensional Reynolds number Re is factored from the viscous flux term.

Numerical Algorithm

The implicit scheme employed in this study is the algorithm reported by Steger et al.[9] The algorithm uses flux-vector splitting[13] and upwind spatial differencing for the convection terms in one coordinate direction (nominally streamwise). As discussed in Ref. 9, schemes using upwind differencing can have several advantages over methods that utilize central spatial differences in each direction. In particular, such schemes can have natural numerical dissipation and better stability properties. By using upwind differencing for the convective terms in the streamwise direction while retaining central differencing in the other directions, a two-factor implicit approximately factored algorithm is obtained, which has been shown to be unconditionally stable[14] for a representative model wave equation. Additional details of the numerical algorithm can be found in Ref. 9.

In the present computations, the flow at the outer boundary of the computational grid was assumed to be the undisturbed freestream. A no-slip condition was applied at the body surface, and a simple zero-axial-gradient extrapolation condition was applied at the downstream end of the computational domain. The flow was assumed to be symmetric about the angle-of-attack plane, and a plane of symmetry condition was used.

Turbulence Model

The coefficients of viscosity and thermal conductivity which appear in Eq. (2) are specified from auxiliary relations. For laminar flow, the coefficient of viscosity is obtained using Sutherland's law, while for turbulent flow the coefficient is obtained from the eddy-viscosity turbulence model reported by Degani and Schiff.[6,7] The coefficient of thermal conductivity is obtained once the viscosity coefficient is known by assuming a constant Prandtl number.

Degani and Schiff developed a modification for high-angle-of-attack flows to the well-known Baldwin-Lomax[11] algebraic model (which is, in turn, based on the two-layer model reported by Cebeci et al.[15]). The modifications extend the model in a rational manner to permit an accurate determination of the viscous length scale for high-angle-of-attack flows in regions of crossflow separation, where a strong leeward vortical flow structure exists.

The rationale for the modifications can be understood if we examine the flow structure on the leeward side of a body at incidence, shown schematically in a crossflow plane in Fig. 1. The flow approaching the line of attachment on the windward plane of symmetry turns and flows circumferentially outward and downstream along the body from the windward toward the leeward side under the action of circumferential pressure gradients. Since the main component of the velocity is along the body, a well-defined boundary layer is developed. The boundary layer separates from the body at ϕ_{S1}, the primary separation line, and the fluid leaves the body along a surface of separation that rolls up to form a primary vortex structure on the leeward side of the body. The primary vortices induce a flow toward the body surface, resulting in a line of attachment at the leeward plane of symmetry. The induced downflow turns and flows circumferentially outward and downstream along the body surface toward the low-pressure region generated by the primary vortices. If the angle of attack of the body is large, and thus the primary vortices sufficiently strong, this induced boundary-layer flow cannot negotiate the adverse circumferential pressure gradient it encounters beyond the low-pressure region of the primary vortex and it separates at ϕ_{S2}, the secondary separation line. The fluid again leaves the body along a surface of separation and rolls up behind the body to form the secondary vortex structure. Another line of attachment is located on the body surface between the primary and secondary separation lines, at $\phi = \phi_A$. Under certain conditions, a tertiary crossflow separation can occur. This would introduce another crossflow separation and attachment line pair located between the attachment line at $\phi = \phi_A$ and the secondary separation line. Thus, the flow is observed to consist of a series of attached boundary layers underlying the leeward-side vortex structure. The vortex structure itself is essentially inviscid and it is dominated by convection of vortical fluid generated within the viscous boundary layer at the body surface rather than by production or dissipation of vorticity along the surfaces of separation. Since the primary direction of the viscous boundary layers is streamwise, it follows that all of these layers should be turbulent when the windward-side boundary layer is turbulent.

As proposed by Baldwin and Lomax,[11] the turbulence model examines a quantity containing the local fluid vorticity magnitude to determine the length scale, and thus the eddy-viscosity coefficient. The modifications made by Degani and Schiff[6,7] permit the model to differentiate between the vorticity within the attached boundary layers from the vorticity on the surfaces of separation, and thus to select a length scale based on the thickness of the attached boundary layers rather than one based on the radial distance between the body surface and the surface of separation. The latter length scale can be much greater than that based on the boundary-layer thickness, and if used, the resulting eddy-viscosity coefficient can be as much as two orders of magnitude too high. In general this will cause the primary vortices to be smaller than those observed experimentally, and the primary separation line will be located closer to the leeward symmetry plane. In addition, the secondary (and tertiary) separation lines will not occur in the computed flows.

The modified turbulence model was developed for high-incidence supersonic flow using a parabolized Navier-Stokes (PNS) code,[8] and was applied to compute numerous high-

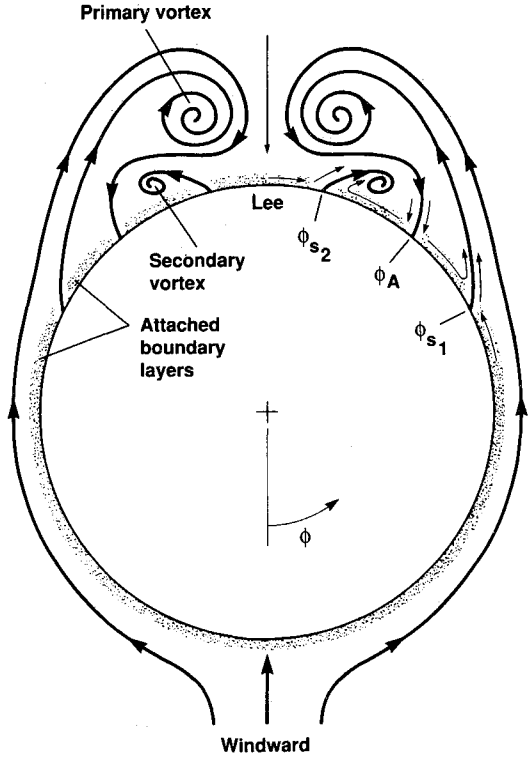

Fig. 1 Schematic of flow structures in crossflow plane.

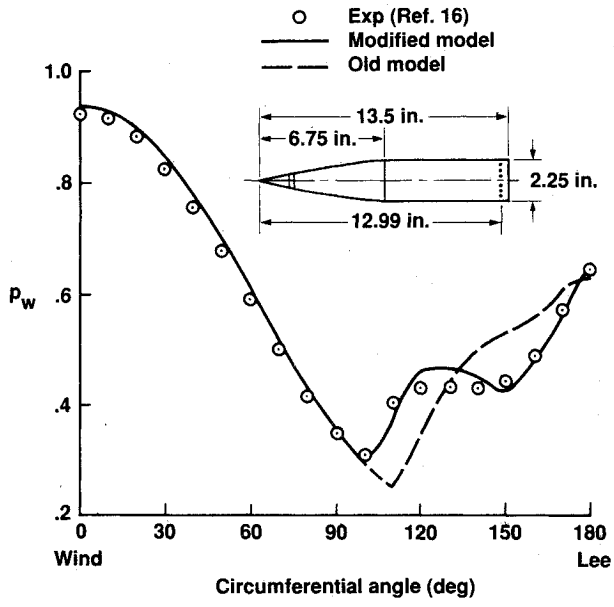

Fig. 2 Circumferential surface pressure distribution on secant-ogive-cylinder at $x/D = 5.77$ [$M_\infty = 3.0$; $\alpha = 10.4$ deg; and $Re_D = 1.22 \times 10^6$ (Ref. 7)].

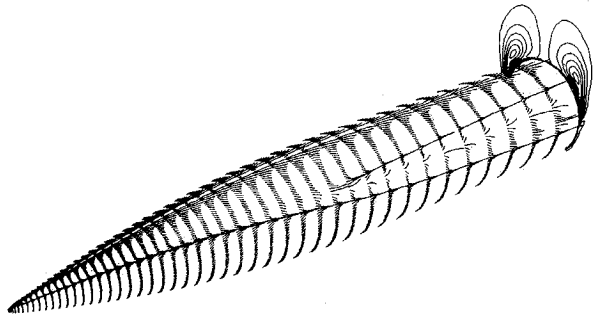

Fig. 3 Surface flow pattern and helicity density contours at $x/D = 6.0$ on ogive-cylinder ($M_\infty = 0.2$; $\alpha = 20$ deg; $Re_D = 200{,}000$; and laminar flow).

alpha supersonic flows about bodies of revolution with success. Figure 2, from Ref. 7, presents computed circumferential pressure distributions obtained at the rear of a secant-ogive-cylinder body at incidence, together with experimental[16] measurements. Figure 2 illustrates the improvement in the prediction of the primary and secondary separations obtained using the modified model, in comparison to the poor results obtained with the unmodified model. The modified model was subsequently adopted to compute a variety of supersonic[1] and, more recently, subsonic[4,5,17] high-incidence flows about bodies with similar success. In this paper, it will be demonstrated why the model carries over so successfully from supersonic to subsonic flows, namely that the physical assumptions on which the model was based are also satisfied in subsonic high-angle-of-attack flows.

Results and Discussion

A series of flows was computed about a tangent ogive-cylinder body in subsonic flow to illustrate the improvements in turbulent flow results due to the modified turbulence model. In these computations, the body had a 3.5 diameter tangent ogive forebody with a cylindrical afterbody extending aft of the nose-body junction for 4.0 diameters. This body geometry had been extensively tested by Lamont[18] in the Ames 12-ft pressure wind tunnel, where detailed surface pressure distributions were obtained at Reynolds numbers ranging from $Re_D = 200{,}000$ to $Re_D = 4.0 \times 10^6$, and at angles of attack ranging from $\alpha = 20$ deg to $\alpha = 90$ deg.

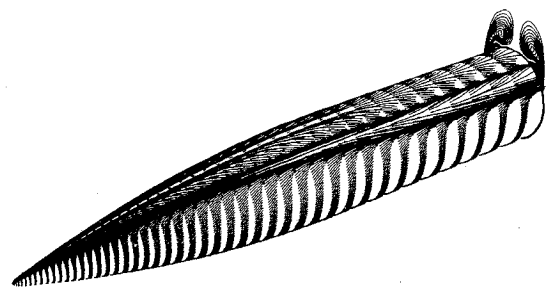

Fig. 4 Surface flow pattern and helicity density contours at $x/D = 6.0$ on ogive-cylinder [$M_\infty = 0.2$; $\alpha = 20$ deg; and turbulent flow (modified model)].

Computations were carried out to predict turbulent flows about the tangent ogive-cylinder body at $M_\infty = 0.2$, and angles of attack of $\alpha = 20$ deg and $\alpha = 30$ deg. Except as noted, all computations were done using the modified[6,7] turbulence model with a fixed cutoff coefficient of 5.0 (see the paragraph "Close Examination of the Flow Structure" for additional details). To eliminate numerical oscillations, the explicit smoothing coefficient was chosen to be 0.02. All numerical results were obtained using a halfbody geometry and a plane-of-symmetry boundary condition. A grid having 59 × 63 × 50 points in the axial, circumferential, and radial directions, respectively, was employed. The nondimensional cylinder diameter was 1.0, and the minimum radial grid spacing, at the body surface, was 0.00001. The grid extended 11 body diameters in the radial direction. Since a zero-gradient extrapolation outflow boundary condition was used, the computed body length was extended 3.0 diameters beyond the physical length of the body to a total of 10.5 diameters to minimize the effect of the outflow boundary. A time-accurate solution was computed starting from freestream initial conditions. This was considered to have converged to a steady-state solution after the ratio of $(L_2\_NORM)/(L_2\_NORM_0)$ of the residual dropped three orders of magnitude.

Subsonic Ogive-Cylinder Flow at $\alpha = 20$ Deg

The computed surface flow pattern for laminar flow ($Re_D = 200{,}000$) at $\alpha = 20$ deg is presented in Fig. 3. Also shown in Fig. 3 are computed helicity density[19] contours in a cross-flow plane at $x/D = 6.0$. It should be noted that the computations were carried out on a body that extended to $x/D = 10.5$. In the experiment of Ref. 18 the body only extended to $x/D = 7.5$, and the last axial station at which measurements were taken was at $x/D = 6.0$. The corresponding computed surface flow pattern and helicity density contours for a fully turbulent case ($Re_D = 4.0 \times 10^6$) is given in Fig. 4.

Note that both the laminar and turbulent flow structures are similar to the one shown schematically in Fig. 1. However, several differences can be observed between the laminar and turbulent flows. In the laminar flow the primary crossflow separation occurs closer to the windward symmetry plane than in the turbulent flow. On the cylinder portion of the body the laminar primary crossflow separation occurs at $\phi \approx 90$ deg, in contrast to $\phi \approx 120$ deg for the turbulent case. This effect is well known from previous experimental investigations of high-incidence body flow, and occurs because the turbulent viscous layer has higher momentum due to increased mixing with the outer inviscid flow, and can thus better negotiate the adverse circumferential pressure gradient it encounters on the leeward side of the body. As a consequence the laminar primary crossflow vortices (shown by the helicity contours) are more widely spaced than in the turbulent flow.

To validate the numerical predictions, a comparison between the computed results and experimental data[18] is made in Figs. 5 and 6. Figure 5 shows computed laminar and turbulent axial surface pressure distributions along the windward plane of symmetry for the solutions shown in Figs. 3 and 4,

together with the surface pressures measured at $\alpha = 20$ deg and $Re_D = 4.0 \times 10^6$. The results show a consistent trend of the experimental measurements of being somewhat higher than the computations on the windward side of the body. It has been suggested that this is the result of the high-angle-of-attack flow condition, in which the windward flow was directed into the pressure taps. Thus the measured pressure was not the surface static pressure, but some combination of the surface static and dynamic pressures.

The analogous comparison for the circumferential surface pressure distributions on the cylindrical portion of the body ($x/D = 6.0$) at $\alpha = 20$ deg is shown in Fig. 6. Note that at this angle of attack the experimental flow remained symmetric, and thus pressures measured on only one side of the body are shown. Figure 6 also shows the circumferential pressure distribution obtained with the unmodified turbulence model. The circumferential pressures are compared in a region of crossflow separation, which is the most difficult region to predict. However, in spite of the complex flow structure, the predictions using the modified model are in good agreement with the experimental data, in contrast to the results of the original Baldwin-Lomax model and the laminar computations.

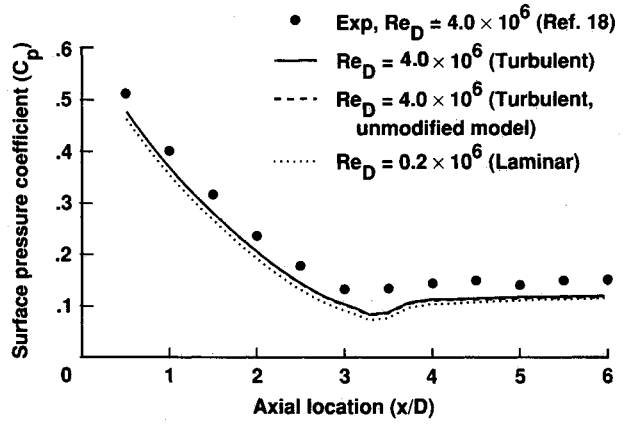

Fig. 5 Computed and measured axial surface pressure distributions along the windward symmetry plane ($M_\infty = 0.2$; $\alpha = 20$ deg; and $Re_D = 4.0 \times 10^6$).

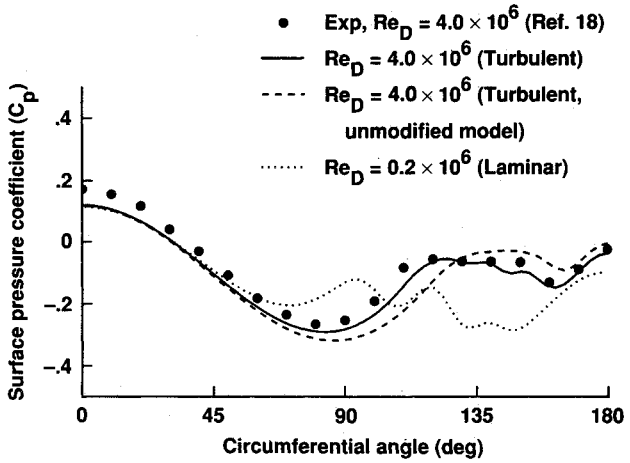

Fig. 6 Computed and measured circumferential surface pressure distributions on the cylindrical portion of the body at $x/D = 6.0$ ($M_\infty = 0.2$; $\alpha = 20$ deg; and $Re_D = 4.0 \times 10^6$).

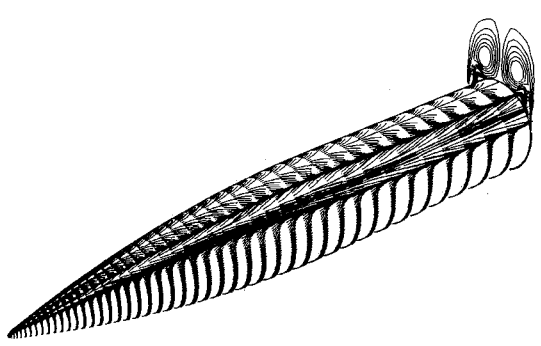

Fig. 7 Surface flow pattern and helicity density contours at $x/D = 6.0$ on ogive-cylinder [$M_\infty = 0.2$; $\alpha = 30$ deg; $Re_D = 3.0 \times 10^6$; and turbulent flow (modified model)].

Subsonic Ogive-Cylinder Flow at $\alpha = 30$ Deg

The computed surface flow pattern for fully turbulent flow at $Re_D = 3.0 \times 10^6$ and $\alpha = 30$ deg is shown in Fig. 7, together with computed helicity density[19] contours in a crossflow plane at $x/D = 6.0$. By comparing Fig. 7 with Fig. 4, it is clearly seen that the size and strength of the leeward-side vortices are much larger at the higher incidence.

The computed circumferential surface pressure distributions on the cylindrical portion of the body at several axial locations are shown in Fig. 8. As was discussed for the case at $\alpha = 20$ deg (Figs. 5 and 6), the computed windward-side pressures are again lower than the experimental measurements, due to the pressure taps measuring a combination of surface static and dynamic pressures.

It is well known that as the angle of attack of a body of revolution is increased, the leeward-side vortex pattern becomes asymmetric. In the present computations, we assumed that the flowfield is symmetric, and the numerical results were obtained using a half-body geometry and a plane-of-symmetry boundary condition. However, experiments[18,20] show that at $\alpha = 30$ deg the flow is asymmetric, and that the extent of the asymmetry increases with further increase in the angle of attack. This asymmetry is shown in Fig. 8 by the experimental surface pressure distributions[18] measured at $\alpha = 30$ deg and $Re_D = 3.0 \times 10^6$. Pressures from both sides of the body are shown, and demonstrate the extent of the asymmetry. For $x/D = 2.0$ and $x/D = 3.5$, the flow is almost symmetric, and the computations match the experimental measurements. For $x/D = 5.0$ and $x/D = 6.0$ where the flow is significantly asymmetric, the computed results lie close to the average of the experimental pressures.

In companion numerical studies of onset of vortex asymmetry in laminar[21,22] and turbulent[17] flows about ogive-cylinders at large incidence, it was found necessary to break the symmetry of the computed solution in order to obtain a stable asymmetric solution. By adding a time-invariant, space-fixed disturbance to the flowfield, a marked asymmetry was obtained in the computed flows. In Ref. 17, by adding a small geometrical disturbance near the nose tip (of about 0.002 of the body diameter) while using the same turbulence model as described here, a good agreement with the experimental measurement was obtained even for $x/D = 6.0$ (see curve in Fig. 8d, taken from Ref. 17).

Close Examination of the Flow Structure

The modified (Degani-Schiff) turbulence model automatically reverts to the Baldwin-Lomax model in regions where there is no overlying vortex structure. Furthermore, it differentiates between regions with attached boundary layers and those with an overlying vortex structure solely on the basis of the local radial flow profiles. This can be seen by examining the details of the flow structure for the ogive-cylinder at $\alpha = 20$ deg shown in Figs. 9–11.

Figure 9 presents a detailed view of the computed helicity density contours in a cross section at $x/D = 6.0$ for the turbulent case at $M_\infty = 0.2$, $\alpha = 20$ deg, and $Re_D = 4.0 \times 10^6$ previously shown in Fig. 4. The solid line separates the primary vortex from the secondary one. The location of the primary and secondary separation lines, and of the attachment lines, are also indicated in Fig. 9. It can be seen that the flow separates at a circumferential angle greater than 90 deg (ϕ_{S1}

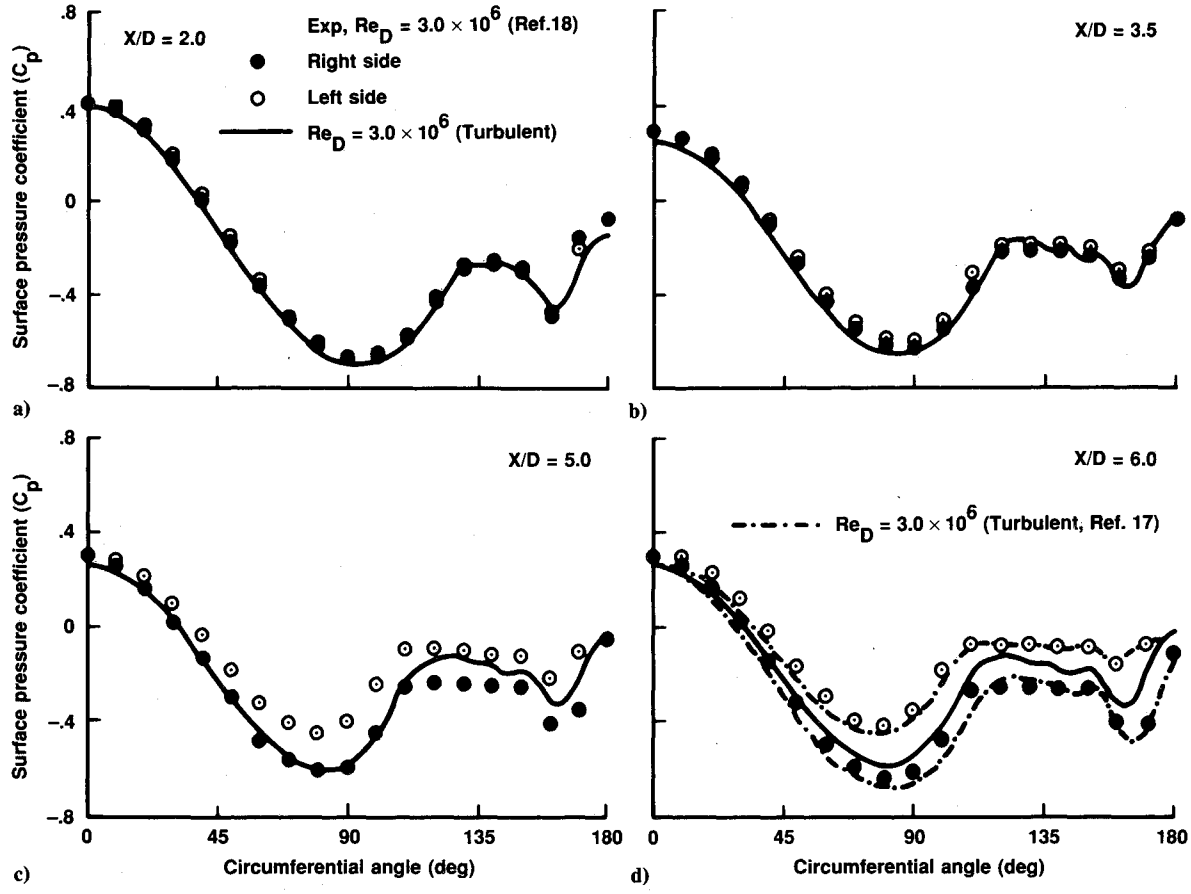

Fig. 8 Computed and measured circumferential surface pressure distributions ($M_\infty = 0.2$; $\alpha = 30$ deg; and $Re_D = 3.0 \times 10^6$).

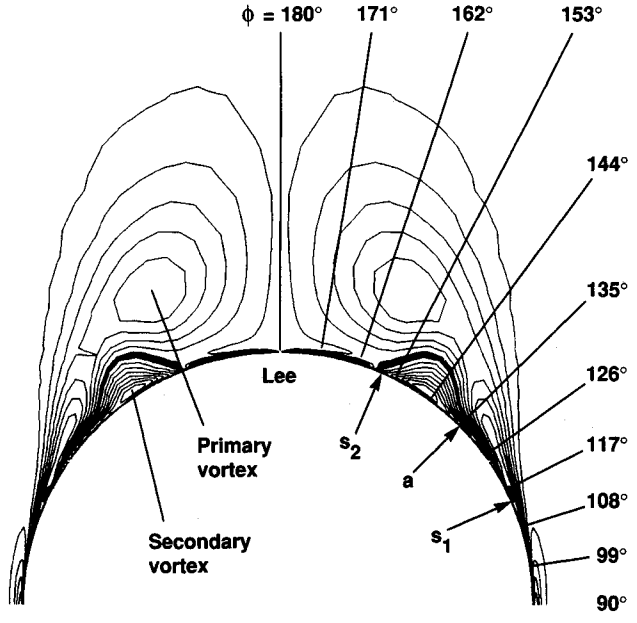

Fig. 9 Helicity density contours in the cross section at $x/D = 6.0$ ($M_\infty = 0.2$; $\alpha = 20$ deg; and $Re_D = 4.0 \times 10^6$).

≈ 113.7 deg) as it should for turbulent flow. As was explained earlier, this computation was carried out using the modified Degani-Schiff[6,7] model, which is based on the Baldwin-Lomax[11] model. In the latter model, the outer layer eddy-viscosity coefficient is based on F_{max}, the maximum value of $F(h)$, which is defined as

$$F(h) = h\,|\omega(h)|\,[1 - e^{-(y^+/A^+)}] \qquad (3)$$

where h is the radial distance above the body, taken in a local profile. Let us now examine several profiles of F, taken along the rays indicated in Fig. 9. These are presented in Fig. 10 as functions of h/D, the radial distance normalized by the cylinder diameter. One should note that the horizontal (h/D) axis is a log scale, which means that actual length of each point is much larger than its appearance in the figure. In Fig. 10, the plots for each angle ϕ can be divided roughly into two groups, those that have only one local maximum (peak) in F and those with more than one local maxima. For example, the profile for $\phi = 0$ deg has only one maximum (at $h/D \approx 2 \times 10^{-3}$); it is characteristic of the behavior of F in attached boundary layers. Here it is easy to determine F_{max} and from it the eddy-viscosity coefficient. Since the flow on the windward side of the body is fully attached, all rays between $\phi = 0$ deg and $\phi = 90$ deg have almost the same form. Also, it can be seen from Fig. 10 that the leeward-ray profile is very similar to that on the windward ray. This should be so, since the flow attaching on the leeward ray has the same total conditions as that impinging on the windward ray. Thus, using the same set of coefficients in the Baldwin-Lomax model would be valid for both the attached windward boundary layer and the leeward boundary layer underlying the vortices.

On the other hand, a profile of F such as the one for $\phi = 135$ deg poses a difficulty. It has two distinct peaks, one due to the boundary layer and the second one due to the vorticity in the vortex above the body. Obviously using the second peak to compute the eddy-viscosity coefficient will result in too large a value (in this example, a value more than two orders of magnitude too large). If this value is used in the computation, the additional viscosity will wash out the details of the vortex structure. The natural step is to stop the search for a maximum of F after the first peak, and that is what is done in the modified model. However, sometimes the decision is not so obvious. For example, consider the profile of F at $\phi = 117$ deg, near the primary separation line, where it

is hard to distinguish between the peaks. A simple way to obtain a value of eddy viscosity in this situation is to sweep sequentially from the windward to the leeward ray, and, for a ray where no distinct peak is found, to use the coefficient obtained from the previous ray. This has the effect of freezing the eddy-viscosity coefficient through the region of the primary crossflow separation, at a value determined in the attached boundary layer on the windward side of the separation line. To accomplish this, two alternative schemes have been employed. In the first, starting from the windward ray, we search for a peak outward along each ray but only up to a cutoff distance chosen as, say, 1.5 times the distance at which the peak in F was found on the previous ray. The reader should note that the axis for radial location, h/D, in Fig. 10 is logarithmic. Thus, the location of the peak due to the vortex for $\phi = 117$ deg, i.e., near the separation, is an order of magnitude larger than the location of peak due to the boundary layer at $\phi = 108$ deg. Therefore, using a factor of 1.5 is usually safe and prevents one from picking the wrong peak due to the presence of the vortex. The second alternative for obtaining the value of eddy viscosity in regions where the peaks in F merge is to use a constant cutoff distance for all rays based on the radial distance of the peak in F found for $\phi = 0$ deg. Such a constant should be determined based on the flow conditions and angle of attack, and usually it should be done by a trial-and-error procedure. In the present work, a constant cutoff distance of 5.0 times the windward ray Y_{max} was used for all calculations. Once two distinct peaks are again found on the leeward side of the separation line, the eddy-

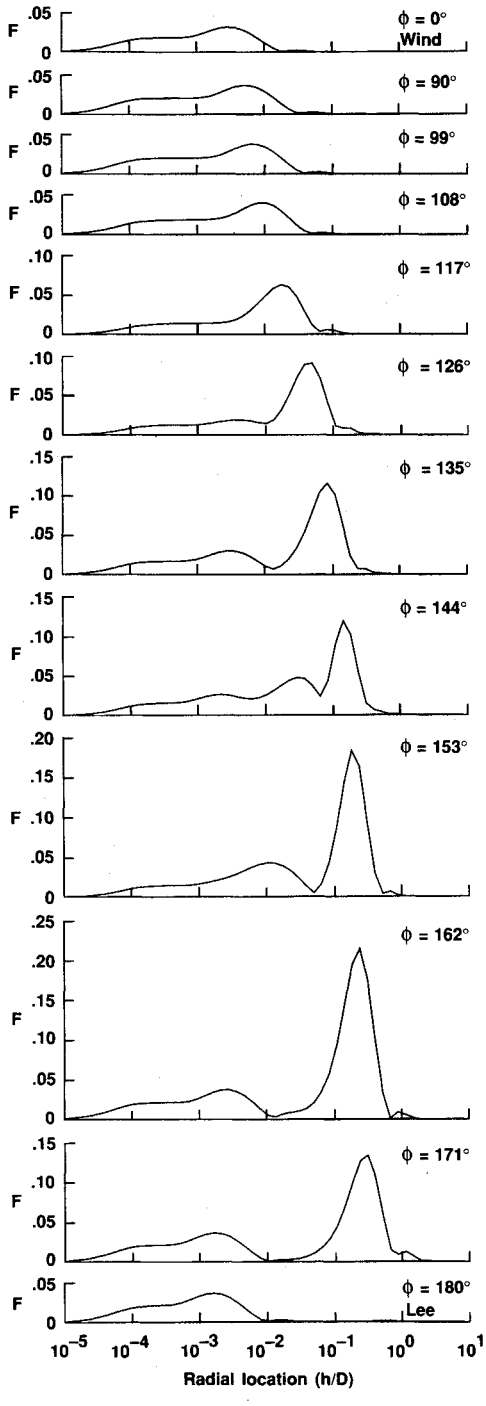

Fig. 10 The F as functions of radial distance above the body surface along the rays shown in Fig. 9 ($M_\infty = 0.2$; $\alpha = 20$ deg; and $Re_D = 4.0 \times 10^6$).

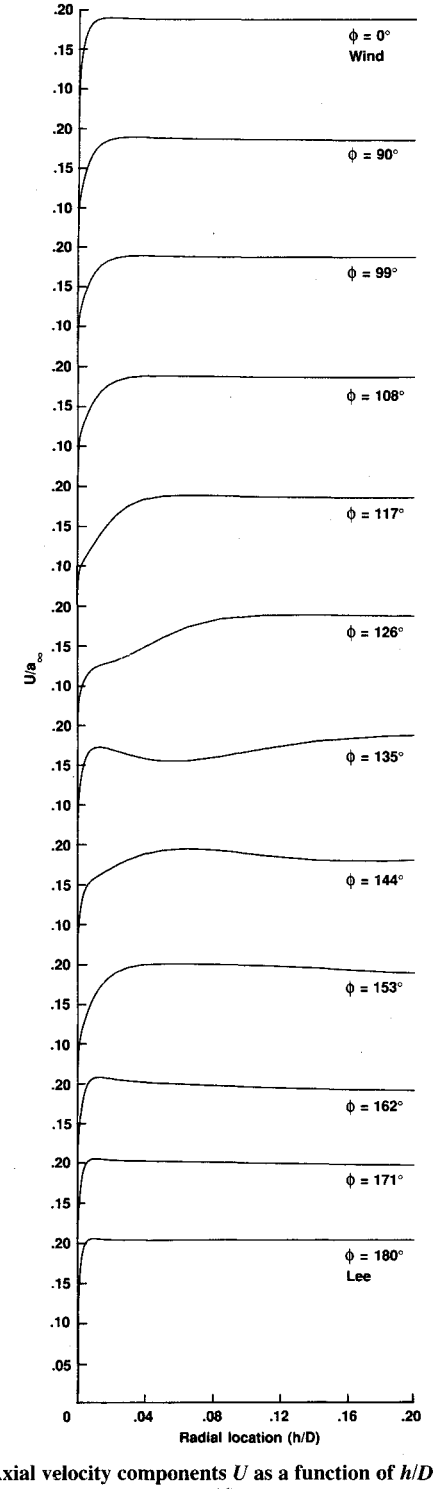

Fig. 11 Axial velocity components U as a function of h/D ($M_\infty = 0.2$; $\alpha = 20$ deg; and $Re_D = 4.0 \times 10^6$).

viscosity coefficient is determined from the boundary layer underlying the free shear layer (vortex feeding sheet).

Freezing the eddy-viscosity coefficient in the vicinity of the crossflow separation line is the weak point of the modified turbulence model. As the circumferential region where freezing occurs increases, so does the uncertainty about the accuracy of the model. For the case at $\alpha = 20$ deg, this region extends circumferentially ≈ 5 deg. However, at $\alpha = 30$ deg, the circumferential extent of this region of uncertainty is smaller, since the leeward vortices are higher above the body, and the shear layers rise above the body surface more rapidly. Thus, despite this approximate treatment of the eddy viscosity in the region of the primary crossflow separation region, for all present cases the model gives results that are in good agreement with experiment, as has been demonstrated by the results of the previous section. Another demonstration of this point is given in Fig. 11, which presents profiles of the axial component of the velocity in the boundary layer. From them one can see that at most circumferential angles on the leeward side of the body (and, although not shown, for all windward-side profiles) the shape of the profile is similar to those found in boundary-layer flows.

It was suggested by Hartwich and Hall[23] that there is a significant difference between subsonic crossflow separations and supersonic ones, and therefore that the turbulence model described above is correct only for supersonic flows and fails in the case of subsonic flows. The main argument that was given in Ref. 23 is that in supersonic cases the surface of separation leaves the body surface at a nonzero angle, while in subsonic cases the flow separates tangentially along the separation line. It was claimed that the Degani-Schiff model "suppresses the close interaction between the tangentially separating vortex feeding sheet and the attached boundary layer."

Hartwich and Hall[23] based their argument about the differences in the leeward flow structure, according to these authors, on a conjecture made by Smith.[24] Careful reading of Smith's paper[24] reveals that indeed in discussing a supersonic flow computation (an inviscid numerical solution by Marconi[25] of flow over a 10-deg half-angle cone) he states that the "spiral stream surface leaves the cone at a nonzero angle." But then Smith goes on to discuss a second supersonic example (flow over a 5-deg half-angle cone) where he mentions "the vortex sheet leaving the surface tangentially and rolling up into a spiral." Obviously the tangential subsonic conjecture does not have too much basis.

Determination of Crossflow Separation Location

Hartwich and Hall[23,26] suggested that for subsonic cases, the Degani-Schiff model should be invoked only in regions of what they called "massive crossflow separation." They determined areas of this massive crossflow separation region by searching from the windward toward the leeward side of the body along a circumferential grid line (at a selected height above the surface, chosen on the basis of zero pressure-gradient flat-plate boundary-layer thickness) for the point where the crossflow velocity changes sign for the first time.

However, it is well known that the crossflow separation line is not located at the point where the crossflow velocity changes sign. The point where the velocity changes sign is dependent on the orientation of the cutting plane (cf. Refs. 3, 7, and 19). It is only reasonably valid when the cutting plane is oriented perpendicular to the line of separation. As illustrated in Fig. 12, even on the cylinder, where the separation line is nearly parallel to the body axis of symmetry, the separation line location does not lie at the point where the crossflow velocity changes sign.

Figure 12 presents several circumferential profiles of the crossflow velocity V_{cir} along circumferential grid lines located at various (constant) heights above the body surface. On each profile, the point where the crossflow velocity first changes sign is indicated by the triangle. In addition, the actual circumferential location of the crossflow separation line at $\phi_{S1} = 113.7$ deg, determined from the surface flow pattern of Fig. 4, is indicated by the vertical line. In all cases, the point where the velocities change sign occurs leeward of the actual separation line location. Furthermore, it is seen that this point varies with the height above the body. In Fig. 12a the change in sign occurs at $\phi \approx 120$ deg, in Fig. 12b it occurs at $\phi \approx 123$ deg, in Fig. 12c it occurs at $\phi \approx 126$ deg, and in Fig. 12d, it occurs at $\phi \approx 129$ deg, all of which are leeward of the actual separation line location. Note that in Fig. 12b, which shows V_{cir} at the height suggested by Hartwich and Hall's criteria for this case, the difference between the actual ϕ_{S1} and the angle where V_{cir} changes sign is more than 9 deg, i.e., more than three circumferential grid points. Moreover, farther forward on the body, where the separation line is not parallel to the body axis, using the change of sign of the crossflow velocity to determine the region of "massive crossflow separation" would be even more arbitrary.

Following Hartwich and Hall's[23,26] suggestion in this instance would lead to using the unmodified Baldwin-Lomax model through the region of crossflow separation, and thus

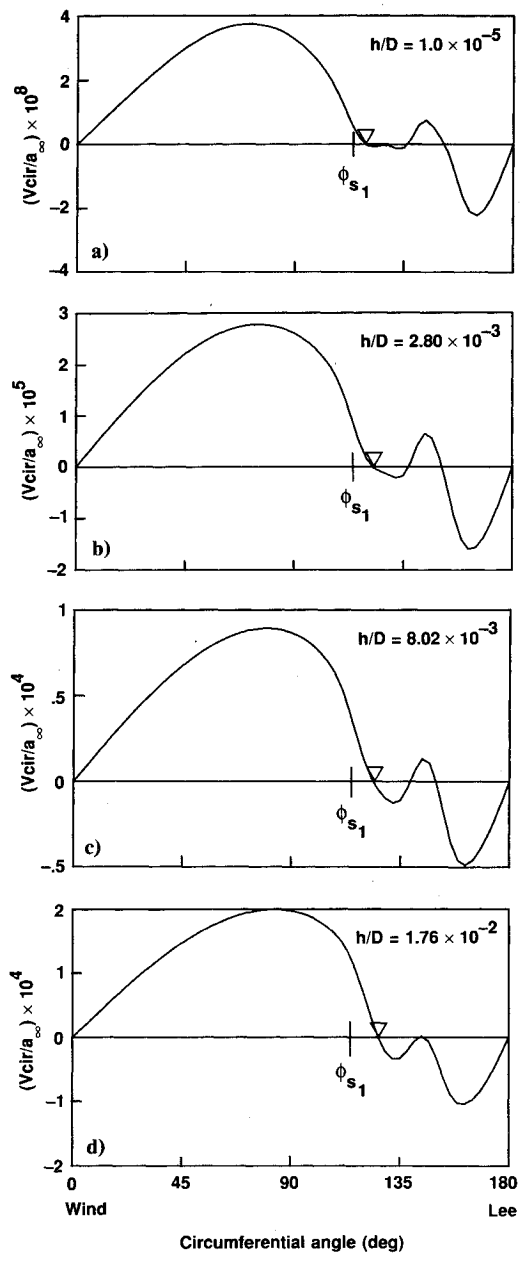

Fig. 12 Crossflow velocities for several values of h/D ($M_\infty = 0.2$; $\alpha = 20$ deg; and $Re_D = 4.0 \times 10^6$).

determining a value of F_{max} due to the vortex and not the one due to the boundary layer. Therefore, the resulting eddy-viscosity coefficient can be as much as two orders of magnitude too large in the most sensitive region of the flow, and the accuracy of the solution would suffer. Selection of the region to apply the Degani-Schiff model on this basis can only arbitrarily restrict its use, but cannot improve its treatment of the region adjoining the crossflow separation line.

Summary

It was demonstrated that the three-dimensional turbulent separated flows and the concentrated vortical structures found in high-angle-of-attack flowfields can be accurately simulated computationally. Predictions have been made for subsonic flow around a geometrically simple body having complex flow structures. The computed results have been shown to be in good agreement with experimental measurements. As demonstrated, searching the profiles of $F(h)$ along rays for local maxima is a rational way of differentiating between the attached boundary layers and the overlying vortical structure. It was shown to work well at $\alpha = 20$ deg, which was chosen for demonstration because the vortices lie close to the body. It works even better at higher angles of attack, where the vortices are located farther above the body, as in the case of subsonic flow at $\alpha = 30$ deg.

The same general flow structure exists for both subsonic and supersonic high-incidence flows, as can be seen by comparing the results shown in Refs. 6 and 7 with those presented here. Moreover, the feeding sheets in the supersonic cases have the same general features as in the subsonic case. Therefore, the claim[23] about the differences between the behavior of feeding sheets of supersonic and subsonic flows is spurious. In view of the similarity between subsonic and supersonic flow, it is not surprising to us that the model works well for all cases with crossflow separation where flow can be considered to be fully turbulent. Furthermore, similar to the solutions of supersonic flow around cones,[6,7] at higher angles of attack the predictions are improved because of the fact that the vortices are located farther above the body.

Lastly, it should be noted that we have treated either fully laminar (i.e., no turbulence model) or fully turbulent flows, both with good success. However, we would expect to find differences between computation and experiment for cases where the actual flow contains large regions of transitional flow, since we have considered the computed flow to be either fully laminar or fully turbulent. The extension of the turbulence model to include a rational transition model is a logical next step.

References

[1]Newsome, R. W., and Adams, M. S., "Numerical Simulation of Vortical Flow Over an Elliptical-Body Missile at High Angles of Attack," AIAA Paper 86-0559, Jan. 1986.

[2]Pan, D., and Pulliam, T. H., "The Computation of Steady Three-Dimensional Separated Flows Over Aerodynamic Bodies at Incidence and Yaw," AIAA Paper 86-0109, Jan. 1986.

[3]Ying, S. X., Schiff, L. B., and Steger, J. L., "A Numerical Study of Three-Dimensional Separated Flow Past a Hemisphere-Cylinder," AIAA Paper 87-1207, June 1987.

[4]Cummings, R. M., Schiff, L. B., Rizk, Y. M., and Chaderjian, N. M., "Numerical Simulation of High-Incidence Flow Over the F-18 Aircraft," International Council of the Aeronautical Sciences Paper 90-3.3.1, Stockholm, Sept. 1990.

[5]Vatsa, V. N., Thomas, J. L., and Wedan, B. W., "Navier-Stokes Computations of Prolate Spheroids at Angle of Attack," AIAA Paper 87-2627, Aug. 1987.

[6]Degani, D., and Schiff, L. B., "Computation of Supersonic Viscous Flows Around Pointed Bodies at Large Incidence," AIAA Paper 83-0034, Jan. 1983.

[7]Degani, D., and Schiff, L. B., "Computation of Turbulent Supersonic Flows Around Pointed Bodies Having Crossflow Separation," *Journal of Computational Physics*, Vol. 66, No. 1, 1986, pp. 173–196.

[8]Schiff, L. B., and Steger, J. L., "Numerical Simulation of Steady Supersonic Viscous Flows," *AIAA Journal*, Vol. 18, No. 12, 1980, pp. 1421–1430.

[9]Steger, J. L., Ying, S. X., and Schiff, L. B., "A Partially Flux-Split Algorithm for Numerical Simulation of Unsteady Viscous Flows," *Proceedings of a Workshop on Computational Fluid Dynamics*, Univ. of California, Davis, CA, 1986.

[10]Viviand, H., "Conservative Forms of Gas Dynamics Equations," *La Recherche Aerospatiale*, Vol. 1, Jan. 1974, pp. 65–68.

[11]Baldwin, B. S., and Lomax, H., "Thin-Layer Approximation and Algebraic Model for Separated Turbulent Flows," AIAA Paper 78-257, Jan. 1978.

[12]Steger, J. L., "Implicit Finite-Difference Simulation of Flow About Arbitrary Two-Dimensional Geometries," *AIAA Journal*, Vol. 16, No. 7, 1978, pp. 679–686.

[13]Steger, J. L., and Warming, R. F., "Flux-Vector Splitting of the Inviscid Gasdynamic Equations with Applications to Finite-Difference Methods," *Journal of Computational Physics*, Vol. 40, No. 2, 1981, pp. 263–293.

[14]Ying, S. X., "Three-Dimensional Implicit Approximately Factored Schemes for Equations in Gasdynamics," Ph.D. Thesis, Stanford Univ., Stanford, CA, June 1986.

[15]Cebeci, T., Smith, A. M. O., and Mosinkis, G., "Calculation of Compressible Adiabatic Turbulent Boundary Layers," *AIAA Journal*, Vol. 8, 1970, pp. 1974–1982.

[16]Reklis, R. P., and Sturek, W. B., "Surface Pressure Measurements on Slender Bodies at Angle of Attack in Supersonic Flow," U.S. Army Ballistic Research Lab., ARRADCOM, Aberdeen Proving Ground, MD, ARBRL-MR-02877, Nov. 1978.

[17]Degani, D., and Levy, Y., "Asymmetric Turbulent Vortical Flows Over Slender Bodies," AIAA Paper 91-3296, Sept. 1991.

[18]Lamont, P. J., "The Complex Asymmetric Flow Over a 3.5D Ogive Nose and Cylindrical Afterbody at High Angles of Attack," AIAA Paper 82-0053, Jan. 1982.

[19]Levy, Y., Degani, D., and Seginer, A., "Graphical Visualization of Vortical Flows by Means of Helicity," *AIAA Journal*, Vol. 28, No. 8, 1990, pp. 1347–1352.

[20]Degani, D., and Zilliac, G. G., "Experimental Study of the Nonsteady Asymmetric Flow Around an Ogive-Cylinder at Incidence," *AIAA Journal*, Vol. 28, No. 4, 1990, pp. 642–649.

[21]Degani, D., and Schiff, L. B., "Numerical Simulation of the Effect of Spatial Disturbances on Vortex Asymmetry," *AIAA Journal*, Vol. 29, No. 3, 1991, pp. 344–352.

[22]Degani, D., "Numerical Investigation of the Origin of Vortex Asymmetry," AIAA Paper 90-0593, Jan. 1990.

[23]Hartwich, P. M., and Hall, R. M., "Navier-Stokes Solutions for Vortical Flows Over a Tangent-Ogive Cylinder," AIAA Paper 89-0337, Jan. 1989.

[24]Smith, J. H. B., "Vortex Flows in Aerodynamics," *Annual Review of Fluid Mechanics*, Vol. 18, 1986, pp. 221–242.

[25]Marconi, F., "The Spiral Singularity in the Supersonic Inviscid Flow Over a Cone," AIAA Paper 83-1665, July 1983.

[26]Hartwich, P. M., and Hall, R. M., "Navier-Stokes Solutions for Vortical Flows Over a Tangent-Ogive Cylinder," *AIAA Journal*, Vol. 28, No. 7, 1990, pp. 1171–1179.